Research, Society and Development, v. 11, n. 16, e104111637755, 2022
(CC BY 4.0) | ISSN 2525-3409 | DOI: http://dx.doi.org/10.33448/rsd-v11i16.37755

Ultrasonic measurements of temperature in materials

Medições ultrassônicas de temperatura em materiais

Mediciones ultrasónicas de temperatura en materiales

Received: 11/10/2022 | Revised: 11/22/2022 | Accepted: 11/23/2022 | Published: 12/01/2022

Patrícia Cardoso de Andrade
ORCID: https://orcid.org/0000-0003-4848-860X
Federal University of Goiás, Brazil
E-mail: patcapatricia@gmail.com
Gilberto de Melo Júnior
ORCID: https://orcid.org/0000-0002-2317-7779
Federal Institute of Education, Science and Technology of Pará, Brazil
E-mail: gilberto.melo@ifpa.edu.br
Sílvio Leão Vieira
ORCID: https://orcid.org/0000-0003-4523-0769
Federal University of Goiás, Brazil
E-mail: slvieira@ufg.br

Abstract
Manufacturing processes and product development for industrial and medical applications are submitted to rigorous quality control. Quality assurance may provide accuracy of the physical quantities concerned to guarantee that defects do not arise when the product is developed. Quantities, such as temperature distribution play a significant role and must be monitored to prevent material damage. However, the number of techniques to sense temperature distribution inside a bulk material in a non-invasive and non-ionizing way is rare. Ultrasonic temperature estimation can overcome this issue, providing an alternative technique that matches such requirements to measure heating within materials. Here, we investigate ultrasonic velocity as a function of temperature in metals, polymers gel to mimic soft tissues (phantom), and biological tissues. Through a customized computational algorithm, we successfully estimated the heat source temperature at the surface, and throughout the length of the material.
Keywords: Temperature distribution; Ultrasound; Thermometry; Velocity; Monitoring.

Resumo
Os processos de fabricação e desenvolvimento de produtos para aplicações industriais e médicas são submetidos a um rigoroso controle de qualidade. A garantia de qualidade pode fornecer precisão das quantidades físicas em questão para garantir que os defeitos não surjam quando o produto for desenvolvido. Quantidades, como distribuição de temperatura, desempenham um papel significativo e devem ser monitoradas para evitar danos materiais. No entanto, o número de técnicas para detectar a distribuição de temperatura no interior de um material de maneira não invasiva e não ionizante é raro. A estimativa de temperatura ultrassônica pode superar esse problema, fornecendo uma técnica alternativa que atende a esses requisitos para medir o aquecimento em materiais. Aqui, investigamos a velocidade ultrassônica em função da temperatura em metais, gel de polímeros para imitar tecidos moles (fantoma) e tecidos biológicos. Por meio de um algoritmo computacional personalizado, estimamos com sucesso a temperatura da fonte de calor na superfície e ao longo do comprimento do material.
Palavras-chave: Distribuição de temperatura; Ultrassom; Termometria; Velocidade; Monitoramento.

Resumen
Los procesos de fabricación y desarrollo de productos para aplicaciones industriales y médicas están sujetos a un estricto control de calidad. El aseguramiento de la calidad puede proporcionar precisión de las cantidades físicas en cuestión para garantizar que no surjan defectos cuando se desarrolle el producto. Las cantidades, como la distribución de la temperatura, juegan un papel importante y deben controlarse para evitar daños materiales. Sin embargo, la cantidad de técnicas para detectar la distribución de temperatura dentro de un material de una manera no invasiva y no ionizante es escasa. La estimación de la temperatura por ultrasonidos puede superar este problema al proporcionar una técnica alternativa que cumple con estos requisitos para medir el calor en los materiales. Aquí, investigamos la velocidad ultrasónica en función de la temperatura en metales, geles poliméricos para imitar tejidos blandos (fantasma) y tejidos biológicos. A través de un algoritmo computacional personalizado, estimamos con éxito la temperatura de la fuente de calor en la superficie y en toda la longitud del material.
Palabras clave: Distribución de temperatura; Ultrasonido; Termometría; Velocidad; Vigilancia.

1. Introduction

Since antiquity, humanity has been dedicated to quantifying the temperature of heated bodies. In engineering and the basic sciences, measuring the internal temperature or temperature gradient in materials is fundamental, especially in manufacturing processes. Many applications use conventional thermocouples (Pollock, 1991) and fiber-optic sensors to measure the temperature (Clegg et al., 1995). However, they are invasive, and it is not always possible to obtain the spatial distribution of the temperature using these thermal sensors. Infrared thermometry is an alternative method for temperature measurement, and it allows thermal monitoring without contact with the medium (Barron, 1992). Measurement using an infrared system is usually affected by different heat sources, which results in measurement inaccuracy. Another limiting factor of infrared techniques is related to depth penetration. Infrared waves have low penetration power in dense materials, making them ineffective for sensing internal temperature measurements in bodies. Lately, measurement of the thermal radiation spectrum emitted from a heated piece of fused silica was done using a computational algorithm to infer the surface's temperature and about tens to hundreds of microns under the surface (Xiao et al., 2020). Therefore, techniques based on thermal radiation are still unable to sense dense materials and metals.

Ultrasonic techniques stand out among the others that can be used to check the temperature of an object. Thus, ultrasound is a potential candidate to monitor temperature distribution because of its ability to probe the interior of large materials and its high sensitivity to temperature dependence (Ihara et al., 2013). Ultrasonic temperature measurement principle is based on the dependence of velocity of sound through the medium with temperature. Such a relation was first reported theoretically in 1873 by Alfred M. Mayer (Afaneh et al., 2011a). The first author to employ ultrasound for temperature monitoring was Gilbert and coauthors in 1985 during an experiment on the cryogenic treatment of hepatocellular carcinoma (Gilbert et al., 1985). Since then, several specific methods of ultrasound thermometry have been proposed (Afaneh et al., 2011b; Bailey et al., 2003; Bharat et al., 2005; Casper et al., 2013; de Oliveira et al., 2010; Konofagou et al., 2002; Lewis et al., 2015; Li et al., 2022; Song et al., 2013; Zhao et al., 2021). Recently, an excellent review covering different ultrasound thermometry methodologies was written by Sinan Li and coauthors (Li et al., 2022), which included enough detail about several modalities that have been proposed in the literature over the past decade. Not long ago, in 2015, Matthew A. Lewis and coauthors analyzed several ultrasound thermometry methods, which include ultrasound B-mode imaging, speckle tracking, thermal deformation, elastography, transverse wave thermometry, local harmonic motion, stimulated acoustic emission, phase contrast, thermoacoustic, and time-of-flight (ToF) (Lewis et al., 2015). Besides these ultrasonic methods, a particular one uses an inverse method based on ToF to solve the thermal diffusion equation. Nevertheless, it will work appropriately if the temperature boundary condition is stable and known during heating. However, depending on the heat source's intensity and location, the thermal boundary condition is often unstable and unknown, for example, in ultrasound hyperthermia (de Tommasi et al., 2021). Another setting can occur when the heat spot is in direct contact with a medium, making it extremely difficult to estimate the material's surface temperature. Therefore, developing an effective method is necessary to overcome such problems and determine the temperature profiles of heated materials quantitatively. In such a way, the inverse analysis method (IAM), coupled with the finite-difference method (FDM) primarily proposed by Ihara, I., and Takahashi, M. has been promising (Ihara et al., 2013).

Here, we explore the IAM, coupled with the FDM, which was used to estimate the heat source's temperature in heated materials through the heat conduction equation's solution. In general, we propose a custom ultrasonic thermometry system, and a new computational algorithm to estimate temperature based on the time-of-flight automatically. A comparison between the ultrasonic temperature measurements was made with conventional thermocouples.

2. Methodology

This section will describe the procedures for obtaining the temperature of material through acoustic waves. Our method is based on boundary conditions measurements, i.e., the heat source at one surface and the opposite temperature at the cold side. To estimate the temperature of the heat source (T_i^{n+1}) is necessary to know the ambient temperature (T_i^1) and material thickness (L). A thermocouple measures the temperature at the material's cold surface, and we use an A-mode ultrasound pulse echo to estimate the thickness. We reference the speed of sound previously known via the calibration curve obtained from the same material sample under test. The calibration curve is also used to obtain a constant (α) by linear regression of the inverse of the velocity of sound as a temperature function and used to estimate the dynamic boundary condition T_i^{n+1}. So, we can indirectly estimate the heat source's temperature at the material surface, which is the focus of our work.

2.1 Ultrasonic wave time-of-flight

The ultrasonic temperature measurement principle is based on the sound velocity's dependence on the temperature. Therefore, the time-of-flight t_L measurement of ultrasonic pulse echoes traveling through the material and as a function of temperature can be determined by:

$$t_L = 2 \int_0^L v(T)^{-1} dx \quad (1)$$

where L represents the material thickness, $v(T)$ the ultrasonic velocity as a function of temperature, schematically, the time-of-flight in the material and its respective graphical representation are shown in Figure 1.

The temperature dependency in the medium is given as a function of position, x, and time, t. The temperature distribution, $T(x, t)$, is subjected to the material thermal boundary condition. Therefore, based on Equation (1), if an appropriate inverse analysis with a defined boundary condition is used, it can be possible to determine the temperature distribution from time-of-flight, t_L measured for the heated medium.

Figure 1 - (a) A pulse-echo ultrasonic wave traveling inside the material, L. (b) The time required for an ultrasonic pulse to travel through the material, t_1, and reflect, t_2, from the back surface or interface.

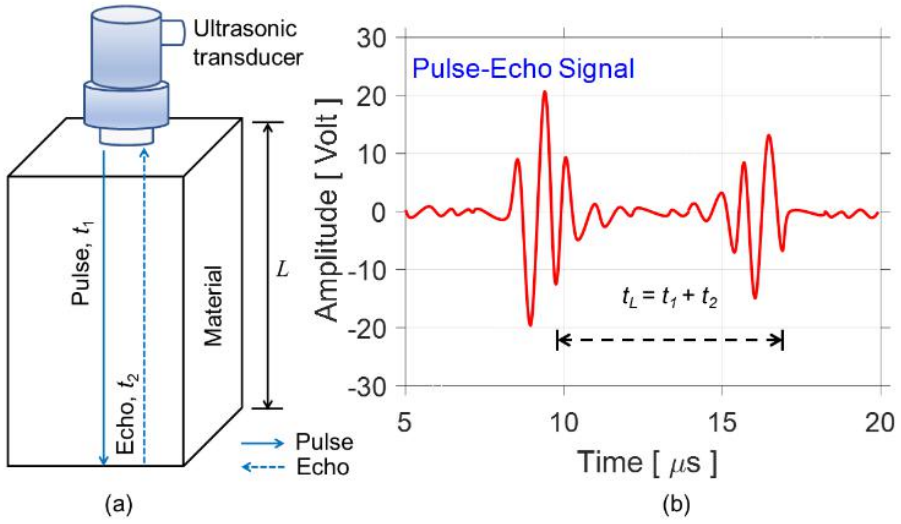

Source: Authors.

2.2 Thermal diffusivity model

One-dimensional heat conduction with constant thermal diffusivity was considered to investigate the temperature distribution. Also, it was assumed that there was no heat source in the block. Thus, the heat conduction equation is given by:

$$\partial T(x,t)/\partial t = \gamma\left(\partial^2 T(x,t)/\partial x^2\right) \quad (2)$$

where γ is the material's thermal diffusivity [m^2/s].

The temperature distribution can be evaluated by solving Equation (2) with well-defined boundary conditions. However, in actual heating processes, the boundary condition is not always kept steady. Typically, such a boundary condition is not simple to predict and even measure. Therefore, determining the temperature distribution from Equation (2) becomes a difficult task. A method capable of evaluating the internal temperature distribution of materials is proposed to solve that problem. The method performs measurements using pulse-echo ultrasound and an inverse analysis coupled with a one-dimensional finite-difference calculation. Thus, one of two boundary conditions is obtained from ultrasonic ToF, and a thermocouple (TC), for example, gives the other in opposition to the heated surface.

2.3 Finite-difference method

The finite-difference method (FDM) or Forward Time Central Space (FTCS) is a numerical method of calculating boundary value problems. The FDM is quite popular because of its simplicity and ease of computational implementation (Gupta, 2019). One of the steps for solving a partial differential equation (PDE) through a numerical method is to discretize the region where the solution is searched. For discretization, a mesh is defined, and the finite set of points belonging to the domain are called nodes of the mesh. A schematic model for the finite-difference method for a single-side heated material with a one-dimensional temperature distribution is illustrated in Figure 2. Where are depicted as an orthogonal Cartesian mesh in which any point (x_i, t_n) is represented in the mesh by (i, n), and the neighbors to this point are represented by $(x_{i\pm1}, t_{n\pm1})$.

Figure 2 - (a) Diagram representation of the experimental setup showing the ultrasonic transducer, the thermocouple, the metal block, and the heat source. (b) Finite-difference discretization of the one-dimensional (1D) heat equation. The FDM approximates the temperature at given grid points, with spacing Δx. The time-evolution is also computed at given times with time step Δt. The solid circles indicate the location of the (known) initial values. The open circles indicate the position of the central points where the finite-difference approximation is computed. The open and solid squares specify the location of the (known) boundary values.

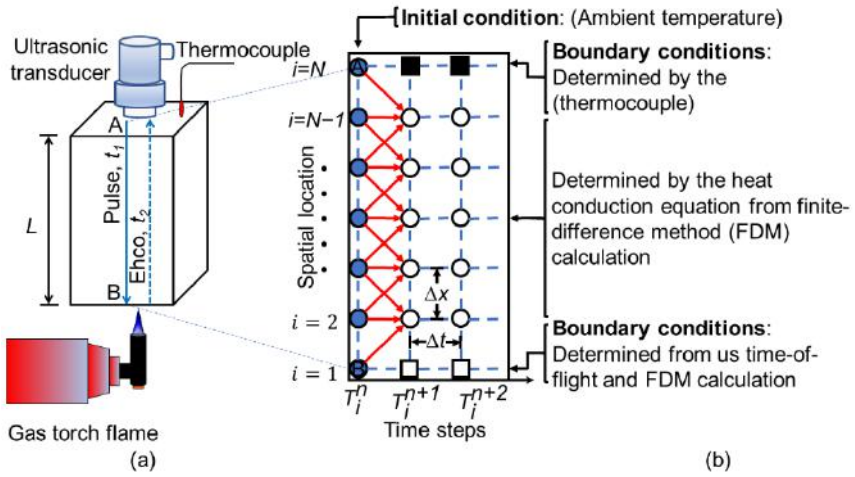

Source: Authors.

The FDM approximates the first and second-order derivatives of the function $T(x, t)$. The centered finite difference of the first-order derivative of the function $T(x, t)$ in space and time, respectively, is given by:

$$\partial T/\partial x \approx (T_{i+1}^{n} - T_{i}^{n})/\Delta x \quad (3)$$

$$\partial T/\partial x \approx \left(T_{i}^{n+1} - T_{i}^{n}\right)/\Delta t \quad (4)$$

The second-order derivative in the diffusivity equation, Equation (3), was derived for the second time, giving

$$\partial^2 T/\partial x^2 \approx (T_{i-1}^{n} - 2T_{i}^{n} + T_{i+1}^{n})/\Delta x^2 \quad (5)$$

One of the steps for solving a second-order partial differential equation is employing a numerical method to discretize the region where the solution is searched. The FDM is a numerical method of calculating big border value problems because of its simplicity and ease of computational implementation. It is based on approximating the first and second-order derivatives of the function *T(x, t)* by the respective first and second-order equation equations in x and t. Figure 2, i, and n are indices corresponding to the spatial and temporal coordinates, respectively, and N is the total number of spatial points in the network. The temperature of each point, i, is given in the network at a time, n; Δt the time interval, and Δx space interval. The index i =1 applies to the heated surface, and $n = N$ is at the opposite surface, T_i^n. In the time interval n =1, only one face of the block is at a given temperature, T^n. The estimated temperature within the metal block in the following steps, $n + 1$, occurs in short time intervals, on the order of a few seconds. So, Equation (5) can be written as:

$$T_{i}^{n+1} = T_{i}^{n} + k(T_{i+1}^{n} + T_{i-1}^{n} - 2T_{i}^{n}) \ \therefore \ (i=2,\ldots, N-1) \quad (6)$$

$$k = \gamma \frac{\Delta t}{\Delta x^2} \quad (7)$$

where Δx is the spatial spacing grid points, and Δt is the time step. The coefficient, k, represents the convergence factor of the Von Neumann equation or stability criterion. Knowing that $k= 0.5$ meets the criterion, this value was adjusted in Equation (7) (Gupta, 2019).

One way to find the terms in Equation (6) is by a recurrence relation, where the next term is a function of the previous one. Since the initial condition (ambient temperature) is given by T_i^l for all i, and T_i^{n+1}, for $i = 2, \ldots, N$-1, must be computed first, and so on.

2.4 Determination of boundary conditions

Temperature boundary conditions are given by the values obtained by a thermocouple (T_N^n,), at the cold surface, and ultrasonic time-of-flight through the material (T_1^{n+1}), at the hot surface (Ihara et al., 2013). The temperature on the heated surface is unknown unless the problem's boundary conditions can be accessed. However, the unknown temperature can be obtained indirectly by ultrasonic time-of-flight in the material and by calculating the finite differences. The use of the ultrasound pulse-echo technique allows us to get a feasible solution to estimate the temperature T_1^{n+1}. Using the trapezoidal rule, we can approach Equation (1) as:

$$t_L = \Delta x\left(v_1^{-1} + v_N^{-1}\right) + 2\Delta x \sum_{i=2}^{N-1} v_i(T)^{-1} \quad (8)$$

Assuming the velocity dependence with temperature inform $v(T) = aT + b$, given in m/s, where a and b are experimental constants obtained by linear regression of data. The inverse of that equation is given by:

$$v_i(T)^{-1} = \alpha T + \beta \tag{9}$$

where α and β have experimentally obtained constants, whose corresponding units are given in [s/m°C] and [s/m], respectively. From Equations (6), (8), and (9), the temperature of the heated surface, T_{n+1}^{l}, in the interval of time $n + 1$, is, therefore:

$$T_1^{n+1} = (t_L^{n+1} - t_L^n)/\alpha\,\Delta x + T_1^n + T_N^n - T_N^{n+1} + 2\sum_{i=2}^{N-1}(T_i^n - T_i^{n+1}) \tag{10}$$

where t_L^n and t_L^{n+1} are the mean time-of-flight in the time steps n and $n + 1$, respectively. Thus, by knowing the time-of-flight of the wave, it was possible to determine the temperature of the heated face in the time interval $n + 1$, where T_1^{n+1} was estimated from Equation (8). Since the temperatures of all points of the network in time step $n + 1$, T_1^{n+1},..., T_N^{n+1}, are determined, the temperature distribution can be evaluated in the next step of time, which is $n + 2$.

2.5 Flowchart of the inverse analysis

The measurement begins with the system estimating the time-of-flight of the ultrasound travel through the material. In the first step, we perform the signal transmission toward and reception from the object. Then, calculate the material thickness by the delay time or time-of-flight between the transmitted and received signal. The material thickness is obtained by multiplying the sound speed by wave time-of-flight and dividing the result by two due to time-of-flight corresponding to a sum of the transmitted time plus the received one. After that, the thickness value is stored on the PC and sent to feed the algorithm's next step, which will compute the discretization mesh to estimate the temperature. The diagram in Figure 3 shows the flowchart of the inverse analysis to determine the temperature distribution.

Figure 3 - Flowchart of the inverse analysis to determine the temperature distribution.

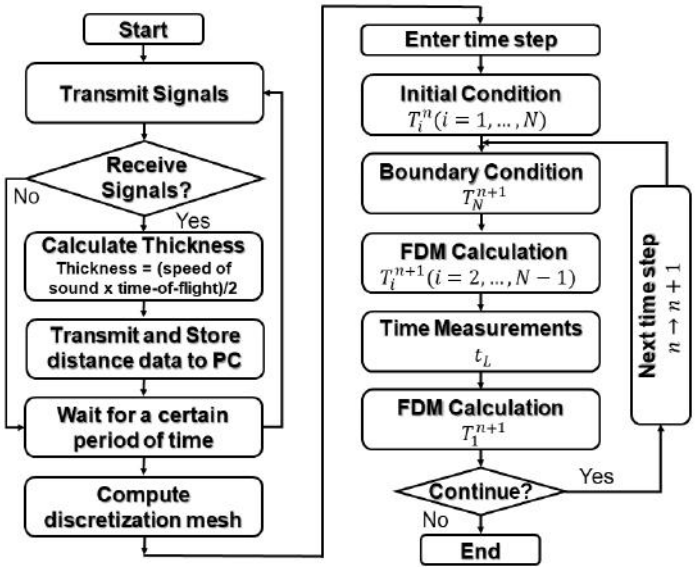

Source: Authors.

The algorithm read the initial temperature of the block by the thermocouple, T_i^1, searching for the initial condition. At each time step was necessary to enter the first boundary condition of the problem, T_N^{n+1}. So, it was possible to calculate the terms T_i^{n+1} (i = 2, ..., N-1) to solve the proposed FDM. Then, the second boundary condition was processed through the ultrasonic time-of-flight and then computed according to Equation (10). Thus, by executing the number of initially ordered temporal steps, the program ends the last data acquisition. It then stops estimating the temperatures of the medium, and the processed data is stored.

2.6 Calibration curve

An experimental setup based on an acoustic water tank (348 ± 1) mm-length, (208 ± 1) mm-width, and (190 ± 1) mm-height was used to evaluate the calibration curve of the model. A thermostatic immersion heater (A100, Lauda-Brinkmann, Lauda, Königshofen, Germany) was employed to control the water temperature. A set of three thermocouples (MTK-01, Minipa, SP, Brazil) were immersed in the bath and used to measure the temperature. The thermocouples were connected to the signal conditioning module (NI DAQ-9212), integrated into the communication module (NI DAQ-9171) from National Instruments, TX, USA, and finally connected to a computer via a USB cable.

We investigate sound speed as a function of temperature in aluminum, gelatin, beef, and bovine liver samples to obtain the system calibration curve. A structural aluminum block (Alloy 7004) of (45.000 ± 0.005) mm-thickness, (25.000 ± 0.005) mm-width, and (31.000 ± 0.005) mm-height was used as standard test material. A phantom simulating soft biological tissue was produced using 15 g of powdered bovine gelatin dissolved in 150 ml of water and 4.5 ml of formaldehyde. It was used to preserve gelatin against bacterial attack and was also used to preserve biological tissue samples. The samples were placed in a cylindrical PVC sample holder of 75 mm in diameter and 25 mm. Tests were carried out in five measurements for each temperature was computed the average and uncertainty. The ultrasonic thermometry system was tested on metallic and non-metallic materials; here, we present the aluminum results.

The time-of-flight in the material was obtained using a 5.0 MHz longitudinal contact ultrasonic transducer with a diameter of 12.7 mm (V110-RM, Panametrics, MA, USA) positioned on the specimens. The accuracy of the measurement of time-of-flight, considering twice the standard deviation, is 7.0 ns. The transducer was connected to a Pulser/Receiver (5072PR, Olympus, PA, USA) via the appropriate coaxial cable. The echo signals acquired are digitized by an oscilloscope (TDS2024C, Tektronix, OR, USA) connected to a PC (Vostro Desktop 3250 SFF, Dell, TX, USA) via a USB interface.

The bath temperature is set initially at 22 °C and increases by 5 °C up to 62 °C. At each step was waited 10 min to guarantee that the system achieved thermal equilibrium. After that, we calculated the speed of sound through the material by the mean of five ultrasonic ToF measurements (de Andrade, 2017; de Andrade & Vieira, 2017, 2018).

2.7 The method of ultrasound thermometry

The ultrasound thermometry method uses the longitudinal contact ultrasonic transducer as a sensing element in the measurement system. The transducer was coupled to the aluminum block's surface by a water-based coupling gel (Biogel, Biomed, SP, Brazil). The material had one side homogeneity heated directly by hot plate heating equipment (NT 103, Novatecnica, SP, Brazil) through pyro ceramic resistance emitting infrared rays of 500 W. The ultrasound transducer was positioned opposite the heated surface. The other sides of the block were covered with special Styrofoam to prevent heat transfer to the air medium.

A thermocouple temperature measurement system was used to verify and validate the TUS method's temperature distribution. This measuring system consisted of two type K thermocouples (MTK-01, Minipa, SP, Brazil) measured in the range

from - 40 to 204 °C with a standard error of 0.75% of the measured value. For example, considering a temperature of 60 °C, one can estimate ± 0.45 °C uncertainty.

The ultrasound thermometry method was verified for different heat sources. The aluminum was subjected to heating using a torch (MT-7706 Micro Torch, Taiwan) followed by cooling. The heat transfer processes were conducted by keeping the heat source 20 mm from the block and 20 s. Two thermocouples (TC1 and TC2) are attached to the heated and cold surface, as shown in the block diagram in Figure 4. The TC2 was fixed on the non-heated surface and used as input for the boundary conditions.

Figure 4 - Representation of the experimental setup.

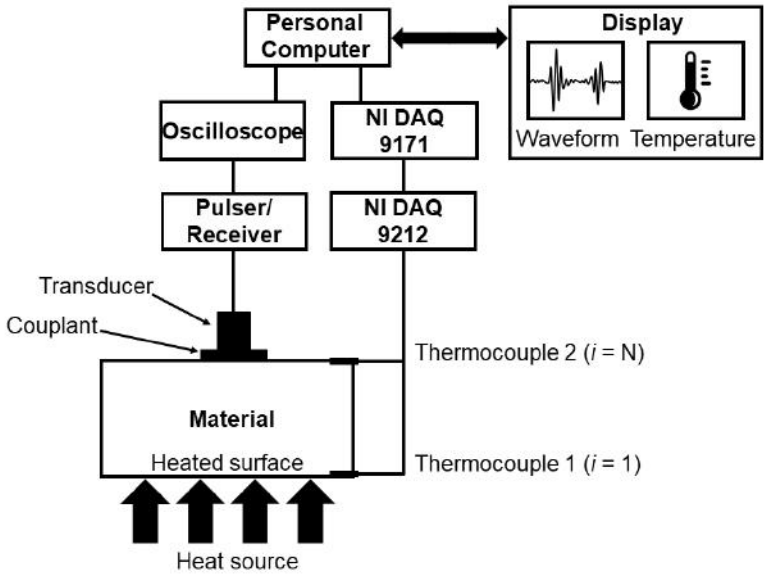

Source: Authors.

The measurements were performed during the block's heating with the oscilloscope at the time base of 2.5 ns. The communication between the instruments and processing of the ultrasonic signals was performed using a custom routine developed in Python (https://www.python.org/) and using Virtual Instrument Software Architecture - VISA (Tektronix, OR, USA). Throughout the measurement process, the collected data could be viewed in real-time for analysis.

Each measurement of the ultrasonic signal was averaged 128 times to minimize fluctuations and noise. It was possible to minimize the uncertainties in the measurements of the time-of-flight by obtaining the mean value. The time-of-flight was obtained by detecting the maximum peak of the first echo. That time was calculated from the time shift of the echo, $t_L = t_L^{n+1} - t_L^n$ during the heating through consecutive steps in the algorithm.

3. Results and Discussion

The relationship between the speed of sound as a function of temperature is depicted in Figures. 5-8. The R-square method was used as a statistical analysis to determine the best fit for the model with 95% confidence bounds. A linear and quadratic fit was applied to the data from samples. Figure 5 shows the relation observed for aluminum, where we can see a decrease in temperature, which is following (Kosugi et al., 2012). The sound speed and temperature uncertainty were obtained by calculating the mean's standard deviation for five repetitions.

Figure 5 - The relation between the speed of sound and the temperature with its associated uncertainty for the aluminum sample.

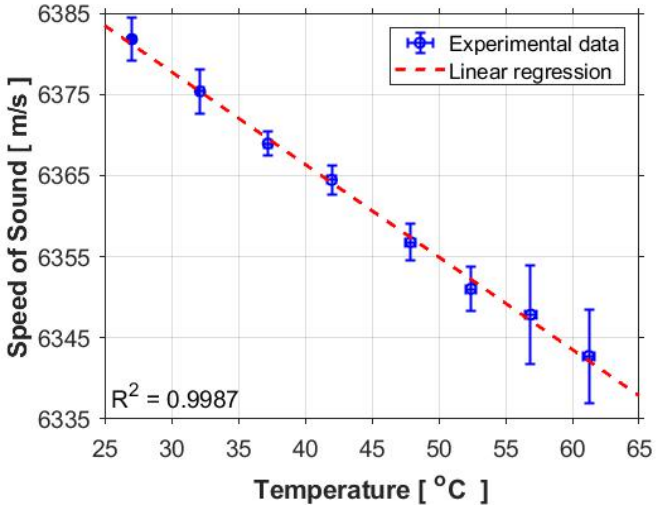

Source: Authors.

The coefficient of determination (R-square) found was 0.9987 From measurements, it was established a characteristic function that represents the calibration curve $v(T) = -(1.14 \pm 0.06)\ T + (6412 \pm 3)$ [m/s]. According to Equation (9), the values of the constants were $\alpha = 2.8317 \times 10^{-10}$ s/cm°C and $\beta = 1.5663 \times 10^{-4}$ s/m.

Figure 6 shows the linear fit of the ultrasonic wave speed as a function of temperature in the gelatin phantom for a temperature range from 30 ºC to 60 ºC.

Figure 6 - The speed of sound versus temperature with its associated uncertainty for the gelatin phantom mimics the mean soft biological tissue velocity.

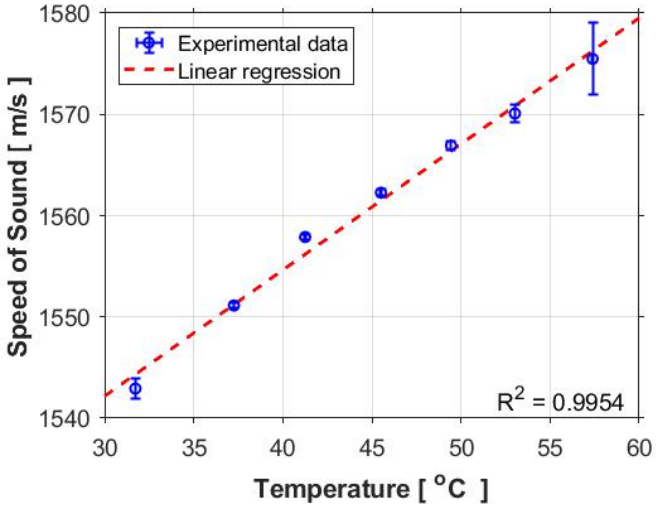

Source: Authors.

Through linear regression, it was found that the data regarding the speed of sound in gelatin showed a strong linear tendency for the studied temperature range. The equation of the adjusted straight line obtained was $v(T) = (1.24 \pm 0.14)\ T + (1505 \pm 3)$ [m/s], with R-square equals to 0.9954; through the linear adjustment, we obtain $\alpha = -2.6101 \times 10^{-8}$ s/cm°C and $\beta = 6.4829 \times 10^{-4}$ s/m.

Figure 7 shows the data points for sound speed as a function of temperature in the fresh bovine liver and its linear fix. It is interesting to note that liver data have a fluctuation around the linear fit. This response is due to the liver tissue's fibrotic nature since it takes five measurements in different places of the sample. The linear equation that best represents that adjustment is found to be $v(T) = (0.46 \pm 0.20)\ T + (1603 \pm 7.5)$ [m/s], with R-square equals to 0.9376; through the linear adjustment, we obtain $\alpha = -7.5666 \times 10^{-9}$ s/cm°C and $\beta = 6.1971 \times 10^{-4}$ s/m.

Figure 7 - The speed of sound and the temperature with its associated uncertainty for the sample of fresh bovine liver.

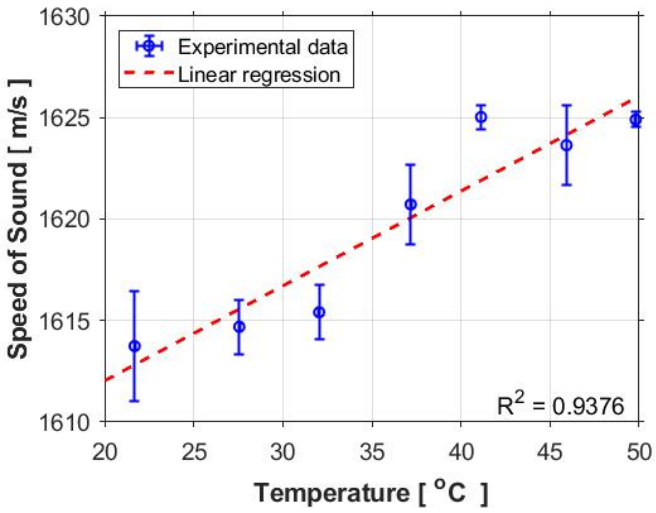

Source: Authors.

Figure 8 shows the relationship between the fresh bovine beef's velocity and the temperature. As we can see in the figure, the data was investigated using a second-order polynomial adjustment for the temperature range of 23 °C to 52 °C, with an R-square of 0.9199.

Figure 8 - the relationship between velocity and temperature with its associated uncertainty for the sample of fresh bovine beef.

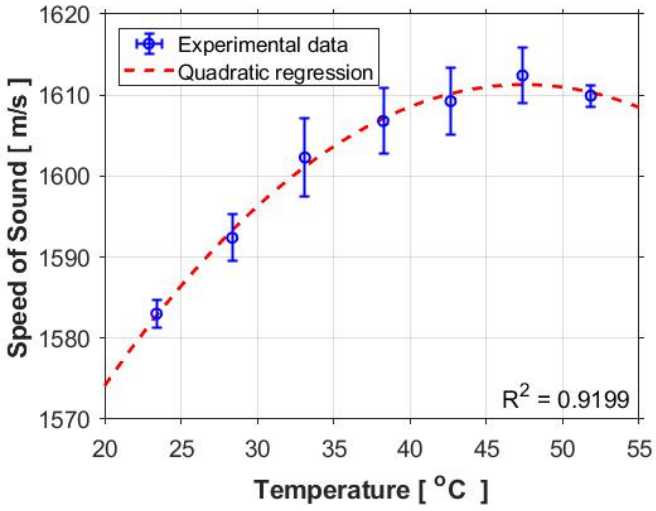

Source: Authors.

It was found that the temperature dependence is approximately given in the quadratic form to be $v(T) = -(0.05 \pm 0.01)\ T^2 + (4.68 \pm 1.1)\ T + (1500 \pm 20)$ [m/s]. However, measurement uncertainties were significant for this temperature range. Thus, verifying that as the temperature increases, the cooking process plays an essential role in increasing the tissue elastic properties, manually observed by touch.

The calibration curve's characterization gave us the experimental constant α, enabling the system to evaluate material gradient temperature distribution. As said, this work focuses on using aluminum as a standard specimen to verify the method's validity. The results from temperature distribution into the aluminum block are depicted in Figure 9.

Because of the quasi-static heating process, the temperature distribution on the block remained uniform over time from 48.78 °C, at time $t = 0$, to about 51.36 °C, at time $t = 80.61$ s. After that, near the heat source, at 5 mm, the temperature begins to change in that loop runtime. Around 12.78 s later, the same situation was observed at the 10th loop, but the block's temperature had risen almost 1.0 °C.

It is essential to point out a general tendency observed in the velocity responses involving the gelatin phantom and the biological tissue of all of them, which have their speed of sound decreasing as a function of temperature. On the other hand, the velocity at the aluminum plate shows inverse behavior, i.e., an increase in the speed of sound as the temperature grows.

Figure 9 - Temperature distribution in the aluminum block over the spatial location for ten runtime steps.

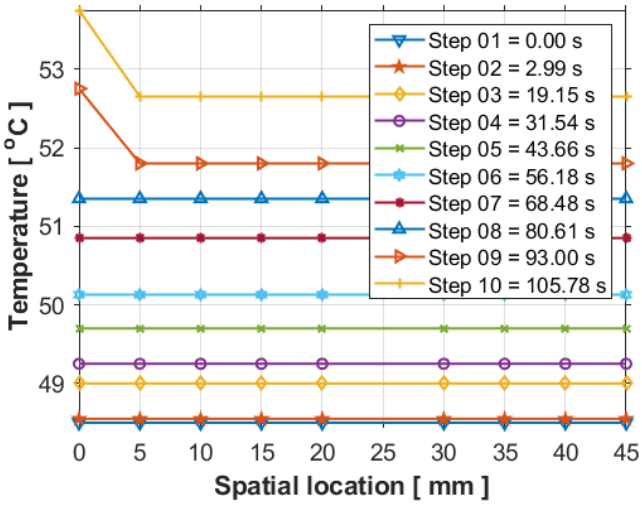

Source: Authors.

In this figure, we notice horizontal lines representing the temperature increase in each loop. They remain partially straight and evenly spaced. This indicates that the temperatures at the block progressively and slowly increased.

Figure 10 are depicted the temporal evaluation of the aluminum block measured on the heated surface and on the non-heated opposite surface obtained by using ultrasound thermometry and thermocouples. The temperature measured in the block, on the hot and cold surfaces, is sensed by different thermocouples, concerning the measurement made with ultrasound on the heated surface. One can see they differ just a bit between them which suggests that the temperature in the entire block increased slowly. This brought the entire length of aluminum into thermal equilibrium before the next temperature rise. The temperature on the aluminum block's heated surface varied from 48.78 °C to 53.70 °C, as shown in Figure 10. In comparison, the thermocouple (TTC) system measured a range from 48.78 °C to 53.00 °C for the same heated surface. From Figure 10, it can be observed that all measurements concerning the temperature difference between these two techniques were lower than 0.70 °C.

Figure 10 - The aluminum block's temperature evolution on the heated surface obtained by both thermometry systems.

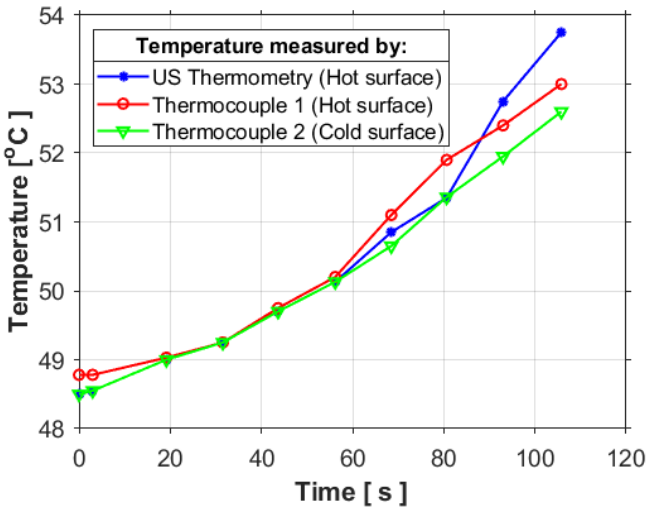

Source: Authors.

The thermocouple used has a standard error limit of ± 2.2 °C or 0.75% of the measured value or uncertainty of ± 0.4 °C. The mean value of the temperature difference obtained by the two techniques was ± 0.12 °C. It indicated a good agreement between both systems to estimate temperature. Similarly, a relatively large fluctuation of about ± 5 °C was found between the temperatures obtained by ultrasound and infrared radiation (Ihara et al., 2013). Other studies point out a standard deviation of the fluctuation of about 2.1 °C (Kosugi et al., 2012).

Table 1 presents the data for the TUS technique's temperature variation for each consecutive step in time. The numerical values of the temperatures on the heated surface, T_1^n. As a function of time for the aluminum block obtained by TUS and TTC, it also shows the temperature difference between these two techniques. The subscribed index number 1 represents the block (heated surface), and *n* is the time step number.

Table 1 - The temperature evaluation on the heated surface of the aluminum block is measured in every temporal loop.

Heated surface temperature variation (°C)
$T_1^2 - T_1^1 = 0.05$
$T_1^3 - T_1^2 = 0.18$
$T_1^4 - T_1^3 = 0.25$
$T_1^5 - T_1^4 = 0.44$
$T_1^6 - T_1^5 = 0.44$
$T_1^7 - T_1^6 = 0.80$
$T_1^8 - T_1^7 = 0.42$
$T_1^9 - T_1^8 = 1.38$
$T_1^{10} - T_1^9 = 0.96$

Source: Authors.

The estimated temperature, T_1^2-T_1^1, refers to the initial temperature variation measured by the TTC and TUS methods after the first-time step. The temperature (T_1^1) is the initial condition obtained by the thermocouple. The average temperature variation between each measured aluminum block's heated surface was 0.42 °C. Meanwhile, the lowest value was 0.18 °C. Temperature measurement using a thermocouple was used as the standard technique, and it was a correlated ultrasonic technique.

Temperature differences below 1 °C were recorded by the two complementary techniques, demonstrating a good agreement between them, which allows quantifying the temperature non-invasive and with no contact directly with the heat source.

The heating using a torch was done, submitting the aluminum to the torch flame for 20 s. Afterward, the aluminum block starts to cool and reaches 39.8 °C after roughly 137.70 s. An elapsed time of 31.54 s is needed to elevate the block's temperature from 35 °C to 102.8 °C, depicted in Figure 11. It shows the temperature profile obtained from time to an aluminum plate of 45 mm thick on the heated surface during the heating and cooling processes.

Figure 11 - Temperature profiling for a 45 mm thick aluminum block, showing the temperature gradient through the center sensed by an ultrasonic transducer.

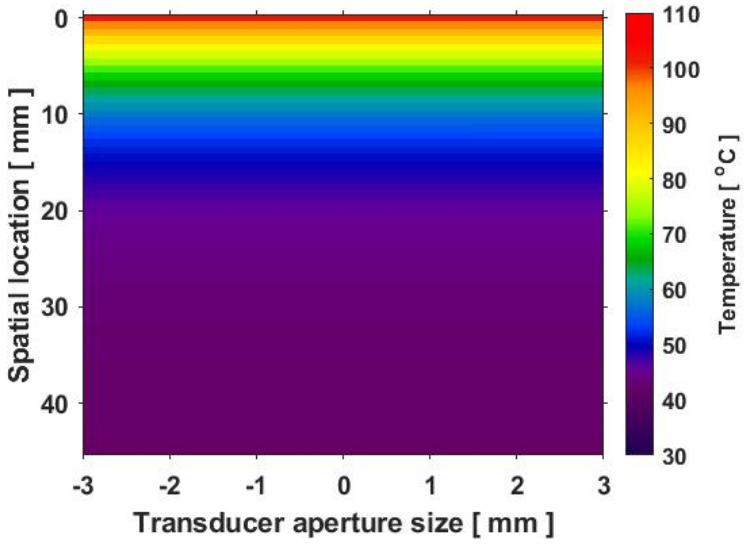

Source: Authors.

The system was not in equilibrium; Ihara and co-authors (Ihara & Takahashi, 2009) early observed discrepancies between ultrasound and thermocouples. However, they could not understand the reason and explain such discrepancies at that moment. To understand the discrepancy between temperatures estimated by both thermometric systems, we investigate possible error sources. One of them was the computational algorithm, but after examining the code, no issue was found. Meanwhile, an interesting phenomenon was observed on the oscilloscope display, independent of data logging. The ultrasonic echo continued to move to the right even after the flame had been turned off. To overcome this question, we examined another aluminum block with less thickness. Suppressively, the temperature difference observed was eliminated when a thinner aluminum plate was used.

Figure 12 shows the temperature profile obtained from time to aluminum of 10 mm thick. Such temperature discrepancies observed in Figure 11 may be related to the phenomenon of thermal inertia. Thermal inertia is defined as the property of a material that expresses the degree of slowness with which its temperature reaches that of the environment [23]. In mechanics, it limits a body's acceleration and uses the relationship between mass and velocity (Kalpakjian, 1992). Similarly, thermal mass and thermal wave velocity are the quantities that control the surface temperature of a material. In the literature, thermal inertia is a function of density, specific heat, and a given material's thermal capacity (Fernández et al., 2005). The figure shows a rapid increase in temperature on one of the faces of the block, reaching a peak around 20 seconds, corresponding to a temperature of 85 °C. Then, the heat source is turned off, and a temperature decay is observed over time. This process was monitored by ultrasound and a thermocouple attached to the heated surface. Simultaneously, on the unheated side, temperature

monitoring was carried out, in which it was observed that there was an average temperature increase, of approximately 1 ºC, with the material initially at a temperature of around 34 ºC.

Figure 12 - Temperature profiling for a 10 mm thick aluminum block for the heated surface during heating and cooling and on the non-heated surface obtained by ultrasound and thermocouples.

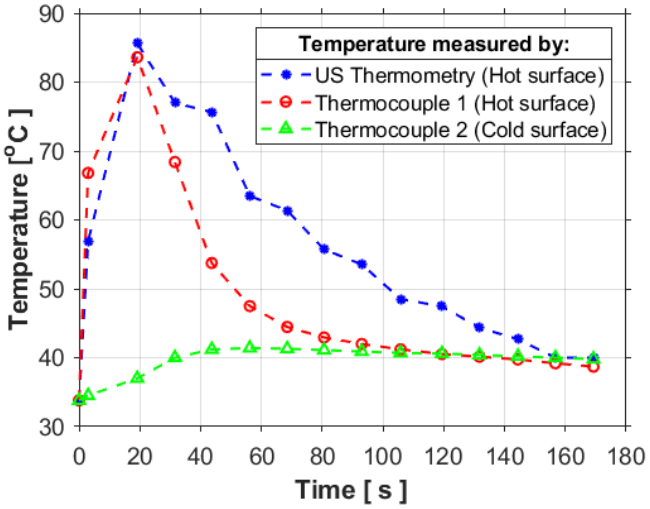

Source: Authors.

So, the thermal capacity characterizes the body, not the substance that constitutes it. It is an extensive property that is proportional to the amount of material present in the body. For example, materials with different heat capacities are constituted by the same substance, even with different masses. For a heat transfer process, a high value of the volumetric thermal capacity means a longer time for the system to reach equilibrium. This behavior is observed in Figure 11 and Figure 12 for two aluminum blocks of distinct thickness subjected to the same heat source and exposure time. The temperature differences may be related to the difference in measurement methods. Similar conduct was previously reported by Soon-Ching Ng and coauthors [23] to predict the inner and outer wall surface temperature of a building over time, recorded at 3 min intervals, 24 h a day for a period of one year.

The system based on the thermocouple has the probe positioned slightly inserted into the aluminum block. Thus, conduction, convection, and radiation cause a rapid loss of the thermometric quantity to the environment. Conversely, ultrasound temperature quantification is dependent on the time-of-flight of the acoustic wave in the medium. This material has a short time-of-flight instead of a large one. Accordingly, the body with high thermal inertia will sense ultrasonic waves even after turning off the heat source at t = 20 s. Experimentally, as said, the phenomenon can be observed on the oscilloscope, where a temporal shift of the reference peak moves to the right until it is stabilized after 15 s (Figure 11), even after the heat source has completely switched off. Experiments conducted with a 10 mm and 1 mm (not shown here) thick aluminum plate decreased that time to less than 5 s (Figure 12) and almost instantly, respectively.

While the cooling process, the temperature difference was less than 9.41 °C and decreased over time. That difference can be related to the thermocouples' effective mass being too small compared to homogeneous aluminum block mass, which can be considered an extension of the ultrasound thermometry probe. The temperature differences are partially related to the thermocouples at the material's surface, where they were not isolated from the medium, which could favor a rapid heat exchange. Most of the time, the temperature estimated by the TUS was higher than those obtained using TTC.

The maximum temperature computed at each depth on the aluminum block during the cooling is presented in Figure 13, where we can see the temperature distribution as a function of the thickness or spatial location. The temperature distribution shown in Figure 13 is from a single transducer element of aperture size 6 mm, considering an RF (radio frequency) signal sampled for one pulse-echo line. According to the barcode in Figure 13, the highest temperature is on top, represented by the red color, corresponding to 102.8 °C. On the bottom, we can see a large area represented by purple, meaning a temperature of 40 °C.

Figure 13 - Temperature distribution represents the maximum temperature computed at each depth on the aluminum block during the cooling.

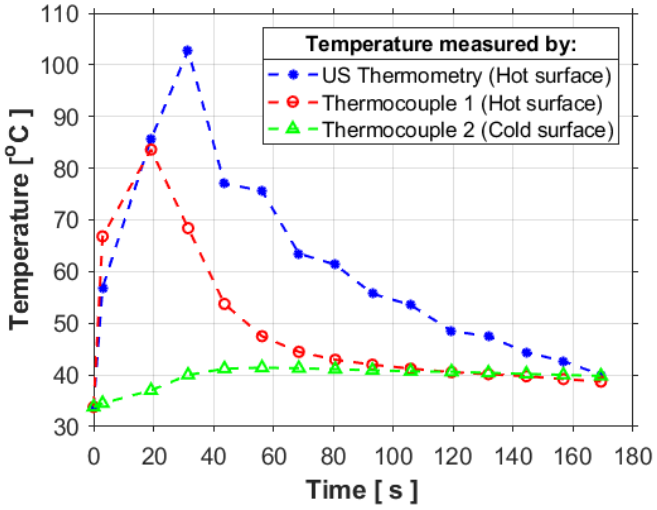

Source: Authors.

The algorithm performs ten computational interactions every 5 mm depth during cooling, registering the block's maximum temperature at 35 s after heating starts. Fitting the one-dimensional temperature distributions (not shown) along the direction of ultrasound propagation inside the heated material using a second-order exponential gave us an R-square of 0.9981. This result indicates an excellent agreement with Newton's law, which states that a body's temperature changes at a rate proportional to the temperature difference between its surroundings.

4. Conclusion

We have described a methodology to estimate the heat source temperature at a heated material surface. As an extension of this method, it can check the internal temperature of heated materials non-invasively. The ultrasound thermometry described herein can predict thermal inertia, also known as "thermal mass", which causes slowness with which its temperature reaches that of the environment over time. Such property is responsible for internal heat storage through the medium for a specific time, which may be a problem in the manufacturing process. Thus, non-invasively estimation of temperature gradients is fundamental and feasible for industrial manufacturing environments. We have used a linear relationship between velocity and temperature as a model for ultrasound thermometry calibration. Indeed, other dependencies like quadratic forms, such as those found in bovine beef, can also be evaluated by determining the quadratic constants and its function's root solution. However, estimating temperature accurately in heterogeneous material, e.g., Biological soft tissue still a challenge to be reached. In that direction, we have made efforts to apply machine learning to help quantify temperature. Significant improvements in temperature estimation

through ultrasonic measurements will be favored with help of artificial intelligence tools, combined with a robust algorithm capable of automatically performing measurements with accuracy for in-situ temperature monitoring.

Acknowledgments

This study was supported by grants from the Brazilian research funding agencies: FAPEG, num. 10267001199-05/2012, CNPq, num. 46229820140-14/2014 and CAPES.

References

Afaneh, A., Alzebda, S., Ivchenko, V., & Kalashnikov, A. N. (2011a). Ultrasonic Measurements of Temperature in Aqueous Solutions: Why and How. *Physics Research International*, *2011*, e156396. https://doi.org/10.1155/2011/156396

Afaneh, A., Alzebda, S., Ivchenko, V., & Kalashnikov, A. N. (2011b). Ultrasonic Measurements of Temperature in Aqueous Solutions: Why and How. *Physics Research International*, *2011*. https://doi.org/10.1155/2011/156396

Bailey, M. R., Khokhlova, V. A., Sapozhnikov, O. A., Kargl, S. G., & Crum, L. A. (2003). Physical mechanisms of the therapeutic effect of ultrasound (a review). *Acoust. Phys.*, *49*(4), 369–388. https://doi.org/10.1134/1.1591291

Barron, W. R. (1992). Principles of Infrared Thermometry. *Sensors Magazine*.

Bharat, S., Techavipoo, U., Kiss, M. Z., Liu, W., & Varghese, T. (2005). Monitoring stiffness changes in lesions after radiofrequency ablation at different temperatures and durations of ablation. *Ultrasound in Medicine & Biology*, *31*(3), 415–422. https://doi.org/10.1016/J.ULTRASMEDBIO.2004.12.020

Casper, A. J., Liu, D., Ballard, J. R., & Ebbini, E. S. (2013). Real-time implementation of a dual-mode ultrasound array system: In vivo results. *IEEE Transactions on Biomedical Engineering*, *60*(10), 2751–2759. https://doi.org/10.1109/TBME.2013.2264484

Clegg, S. T., Das, S. K., Zhang, Y., Macfall, J., Fullar, E., & Samulski, T. V. (1995). Verification of a hyperthermia model method using MR thermometry. *International Journal of Hyperthermia*. https://doi.org/10.3109/02656739509022476

de Andrade, P. C. (2017). *Desenvolvimento de um sistema de termometria por ultrassom para monitoramento de temperatura em materiais* [Dissertação]. Universidade Federal de Goiás.

de Andrade, P. C., & Vieira, S. L. (2017). Monitoramento de temperatura interna em materiais por termometria ultrassônica. *Revista Brasileira de Física Médica*, *11*(2), 34–37. https://doi.org/10.29384/rbfm.2017.v11.n2.p34-37

de Andrade, P. C., & Vieira, S. L. (2018). Development of an ultrasonic thermometry system. *IEEE Latin America Transactions*, *16*(6). https://doi.org/10.1109/TLA.2018.8444385

de Oliveira, P. L., de Senneville, B. D., Dragonu, I., & Moonen, C. T. W. (2010). Rapid motion correction in MR-guided high-intensity focused ultrasound heating using real-time ultrasound echo information. *NMR Biomed.*, *23*(9), 1103–1108. https://doi.org/10.1002/nbm.1526

de Tommasi, F., Massaroni, C., Grasso, R. F., Carassiti, M., & Schena, E. (2021). Temperature Monitoring in Hyperthermia Treatments of Bone Tumors: State-of-the-Art and Future Challenges. *Sensors 2021, Vol. 21, Page 5470*, *21*(16), 5470. https://doi.org/10.3390/S21165470

Fernández, J. L., Porta-Gándara, M. A., & Chargoy, N. (2005). Rapid on-site evaluation of thermal comfort through heat capacity in buildings. *Energy and Buildings*. https://doi.org/10.1016/j.enbuild.2004.09.003

Gilbert, J. C., Onik, G. M., Hoddick, W. K., & Rubinsky, B. (1985). Real time ultrasonic monitoring of hepatic cryosurgery. *Cryobiology*. https://doi.org/10.1016/0011-2240(85)90179-8

Gupta, R. K. (2019). Partial Differential Equations: Finite Difference Methods. In *Numerical Methods: Fundamentals and Applications*. https://doi.org/10.1017/9781108685306.017

Ihara, I., & Takahashi, M. (2009). Ultrasound thermometry for monitoring internal temperature gradient in heated material. *Proceedings - IEEE Ultrasonics Symposium*. https://doi.org/10.1109/ULTSYM.2009.5441882

Ihara, I., Tomomatsu, T., Takahashi, M., Kosugi, A., Matsuya, I., & Yamada, H. (2013). *Ultrasonic Thermometry for Temperature Profiling of Heated Materials*. https://doi.org/10.1007/978-3-642-32180-1_13

Kalpakjian, S. and S. R. S. (1992). *Manufacturing Processes for Engineering Materials* (2nd Ed). Addison-Wesley Publishing Company.

Konofagou, E. E., Thierman, J., Karjalainen, T., & Hynynen, K. (2002). The temperature dependence of ultrasound-stimulated acoustic emission. *Ultrasound in Medicine & Biology*, *28*(3), 331–338. https://doi.org/10.1016/S0301-5629(01)00525-7

Kosugi, A., Ihara, I., & Matsuya, I. (2012). Accuracy evaluation of surface temperature profiling by a laser ultrasonic method. *Japanese Journal of Applied Physics*. https://doi.org/10.1143/JJAP.51.07GB01

Lewis, M. A., Staruch, R. M., & Chopra, R. (2015). Thermometry and ablation monitoring with ultrasound. In *International Journal of Hyperthermia*. https://doi.org/10.3109/02656736.2015.1009180

Li, S., Zhou, Z., Wu, S., & Wu, W. (2022). A Review of Quantitative Ultrasound-Based Approaches to Thermometry and Ablation Zone Identification Over the Past Decade. *Ultrasonic Imaging*. https://doi.org/10.1177/01617346221120069/FORMAT/EPUB

Pollock, D. D. (1991). Thermocouples: Theory and Properties. *Boca Raton, FL: CRC Press*.

Song, J. H., Yoo, Y., Song, T. K., & Chang, J. H. (2013). Real-time monitoring of HIFU treatment using pulse inversion. *Physics in Medicine & Biology*, *58*(15), 5333. https://doi.org/10.1088/0031-9155/58/15/5333

Xiao, Y., Wan, C., Shahsafi, A., Salman, J., & Kats, M. A. (2020). Depth Thermography: Noninvasive 3D Temperature Profiling Using Infrared Thermal Emission. *ACS Photonics*. https://doi.org/10.1021/acsphotonics.9b01588

Zhao, L., Zhou, X., Dong, C., Wu, Y., & Wang, H. (2021). Ultrasonic Thermometry Algorithm Based on Inverse Quadratic Function. *IEEE Transactions on Ultrasonics, Ferroelectrics, and Frequency Control*, *68*(5), 1876–1884. https://doi.org/10.1109/TUFFC.2020.3036116